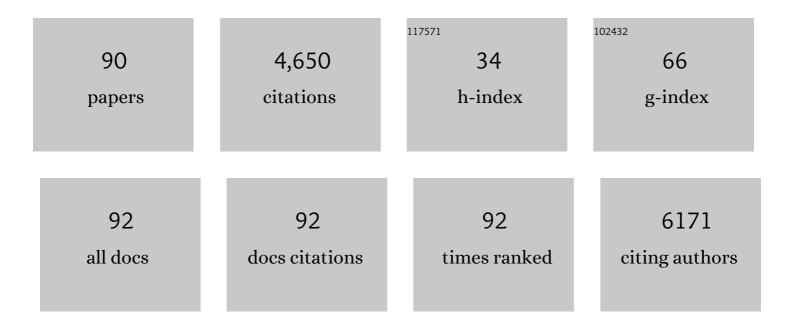
List of Publications by Year in descending order

Source: https://exaly.com/author-pdf/5427261/publications.pdf Version: 2024-02-01



#	Article	IF	CITATIONS
1	Synthesis of Carbon–Metal Oxide Composites as Catalyst Supports by "Cooking Sugar with Salt― ACS Sustainable Chemistry and Engineering, 2022, 10, 731-737.	3.2	3
2	Highly efficient and selective electrocatalytic hydrogen peroxide production on Co-O-C active centers on graphene oxide. Communications Chemistry, 2022, 5, .	2.0	33
3	Direct Synthesis of Stable 1Tâ€MoS ₂ Doped with Ni Single Atoms for Water Splitting in Alkaline Media. Small, 2022, 18, e2107238.	5.2	58
4	Surface Ligand Tuning of Coordination Geometry and Pb 6s ² Electronic Pair Stereochemical Activity in MAPbBr ₃ Perovskite Nanoparticles: A Joint Experimental and Theoretical Insight. Journal of Physical Chemistry C, 2022, 126, 7500-7509.	1.5	4
5	Decreasing the Overpotential of Aprotic Liâ€CO ₂ Batteries with the Inâ€Plane Alloy Structure in Ultrathin 2D Ruâ€Based Nanosheets. Advanced Functional Materials, 2022, 32, .	7.8	39
6	Aqueous Electrolytes with Hydrophobic Organic Cosolvents for Stabilizing Zinc Metal Anodes. ACS Nano, 2022, 16, 9667-9678.	7.3	126
7	Experimental and Theoretical Insights into Enhanced Hydrogen Evolution over PtCo Nanoalloys Anchored on a Nitrogen-Doped Carbon Matrix. Journal of Physical Chemistry Letters, 2022, 13, 5195-5203.	2.1	7
8	Approach to electrochemical modulating differential extended X-ray absorption fine structure. Journal of Synchrotron Radiation, 2022, 29, 1065-1073.	1.0	5
9	<i>Operando</i> X-ray spectroscopy visualizing the chameleon-like structural reconstruction on an oxygen evolution electrocatalyst. Energy and Environmental Science, 2021, 14, 906-915.	15.6	93
10	Precise fabrication of single-atom alloy co-catalyst with optimal charge state for enhanced photocatalysis. National Science Review, 2021, 8, nwaa224.	4.6	125
11	A new type of noncovalent surface–π stacking interaction occurring on peroxide-modified titania nanosheets driven by vertical π-state polarization. Chemical Science, 2021, 12, 4411-4417.	3.7	13
12	Understanding the Mesoscale Degradation in Nickel-Rich Cathode Materials through Machine-Learning-Revealed Strain–Redox Decoupling. ACS Energy Letters, 2021, 6, 687-693.	8.8	42
13	Magnetic Particles Unintentionally Emitted from Anthropogenic Sources: Iron and Steel Plants. Environmental Science and Technology Letters, 2021, 8, 295-300.	3.9	15
14	Solvent coordination engineering for high-quality hybrid organic-inorganic perovskite films. Journal of Materials Science, 2021, 56, 9903-9913.	1.7	6
15	A polarization-switch effect of silicon crystals under multiple-beam diffraction geometry. Journal of Applied Crystallography, 2021, 54, 976-981.	1.9	2
16	Sulfur stabilizing metal nanoclusters on carbon at high temperatures. Nature Communications, 2021, 12, 3135.	5.8	104
17	Highly Selective Oxidation of Methane into Methanol over Cu-Promoted Monomeric Fe/ZSM-5. ACS Catalysis, 2021, 11, 6684-6691.	5.5	73
18	Atomic Structural Evolution of Single‣ayer Pt Clusters as Efficient Electrocatalysts. Small, 2021, 17, e2100732.	5.2	26

#	Article	IF	CITATIONS
19	Architecting Freestanding Sulfur Cathodes for Superior Roomâ€Temperature Na–S Batteries. Advanced Functional Materials, 2021, 31, 2102280.	7.8	46
20	Application of Xâ€Ray Absorption Spectroscopy in Electrocatalytic Water Splitting and CO ₂ Reduction. Small Science, 2021, 1, 2100023.	5.8	16
21	Zeoliteâ€Tailored Active Site Proximity for the Efficient Production of Pentanoic Biofuels. Angewandte Chemie - International Edition, 2021, 60, 23713-23721.	7.2	43
22	Zeoliteâ€Tailored Active Site Proximity for the Efficient Production of Pentanoic Biofuels. Angewandte Chemie, 2021, 133, 23906-23914.	1.6	10
23	Microporous Sulfur-Doped Carbon Atoms as Supports for Sintering-Resistant Platinum Nanocluster Catalysts. ACS Applied Nano Materials, 2021, 4, 9489-9496.	2.4	9
24	Sulfur-anchoring synthesis of platinum intermetallic nanoparticle catalysts for fuel cells. Science, 2021, 374, 459-464.	6.0	343
25	Identification of Catalytic Sites for Oxygen Reduction in Metal/Nitrogenâ€Đoped Carbons with Encapsulated Metal Nanoparticles. Angewandte Chemie - International Edition, 2020, 59, 1627-1633.	7.2	176
26	Identification of Catalytic Sites for Oxygen Reduction in Metal/Nitrogenâ€Doped Carbons with Encapsulated Metal Nanoparticles. Angewandte Chemie, 2020, 132, 1644-1650.	1.6	138
27	Innenrücktitelbild: Identification of Catalytic Sites for Oxygen Reduction in Metal/Nitrogenâ€Đoped Carbons with Encapsulated Metal Nanoparticles (Angew. Chem. 4/2020). Angewandte Chemie, 2020, 132, 1759-1759.	1.6	0
28	High-Temperature Synthesis of Small-Sized Pt/Nb Alloy Catalysts on Carbon Supports for Hydrothermal Reactions. Inorganic Chemistry, 2020, 59, 15953-15961.	1.9	7
29	Rational design of hierarchical FeSe ₂ encapsulated with bifunctional carbon cuboids as an advanced anode for sodium-ion batteries. Nanoscale, 2020, 12, 22210-22216.	2.8	26
30	A library of carbon-supported ultrasmall bimetallic nanoparticles. Nano Research, 2020, 13, 2735-2740.	5.8	18
31	Synthesis of carbon-supported sub-2 nanometer bimetallic catalysts by strong metal–sulfur interaction. Chemical Science, 2020, 11, 7933-7939.	3.7	17
32	Prediction of topological nontrivial semimetals and pressure-induced Lifshitz transition in 1T′-MoS ₂ layered bulk polytypes. Nanoscale, 2020, 12, 22710-22717.	2.8	8
33	Activation of subnanometric Pt on Cu-modified CeO2 via redox-coupled atomic layer deposition for CO oxidation. Nature Communications, 2020, 11, 4240.	5.8	101
34	Cationâ^'Ï€ Interactions with Coexisting Heavy Metals Enhanced the Uptake and Accumulation of Polycyclic Aromatic Hydrocarbons in Spinach. Environmental Science & Technology, 2020, 54, 7261-7270.	4.6	22
35	Highly dispersed Pt studded on CoO _x nanoclusters for CO preferential oxidation in H ₂ . Journal of Materials Chemistry A, 2020, 8, 10180-10187.	5.2	21
36	[MW ₁₂ O ₄₄] clusters: unprecedented central heteroatoms atomically dispersed in the eight coordination state bridging the 1 : 12 polyoxometalate family of Keggin and Silverton. Nanoscale, 2019, 11, 22270-22276.	2.8	9

#	Article	IF	CITATIONS
37	Hierarchically porous carbons as supports for fuel cell electrocatalysts with atomically dispersed Fe–N _x moieties. Chemical Science, 2019, 10, 8236-8240.	3.7	34
38	Reversing the charge transfer between platinum and sulfur-doped carbon support for electrocatalytic hydrogen evolution. Nature Communications, 2019, 10, 4977.	5.8	243
39	A sulfur-tethering synthesis strategy toward high-loading atomically dispersed noble metal catalysts. Science Advances, 2019, 5, eaax6322.	4.7	177
40	A metal-catalyzed thermal polymerization strategy toward atomically dispersed catalysts. Chemical Communications, 2019, 55, 11579-11582.	2.2	8
41	Sub-2 nm Ir Nanoclusters Immobilized on Mesoporous Nitrogen-Doped Carbons as Efficient Catalysts for Selective Hydrogenation. ACS Applied Nano Materials, 2019, 2, 6546-6553.	2.4	20
42	Switching Co/N/C Catalysts for Heterogeneous Catalysis and Electrocatalysis by Controllable Pyrolysis of Cobalt Porphyrin. IScience, 2019, 15, 282-290.	1.9	20
43	Nickel catalyst with atomically-thin meshed cobalt coating for improved durability in dry reforming of methane. Journal of Catalysis, 2019, 373, 351-360.	3.1	42
44	Photoelectric conversion on Earth's surface via widespread Fe- and Mn-mineral coatings. Proceedings of the National Academy of Sciences of the United States of America, 2019, 116, 9741-9746.	3.3	111
45	One-pot synthesis of porous 1T-phase MoS2 integrated with single-atom Cu doping for enhancing electrocatalytic hydrogen evolution reaction. Applied Catalysis B: Environmental, 2019, 251, 87-93.	10.8	160
46	Improved NO–CO reactivity of highly dispersed Pt particles on CeO ₂ nanorod catalysts prepared by atomic layer deposition. Catalysis Science and Technology, 2019, 9, 2664-2672.	2.1	34
47	Pressure induced transformation and subsequent amorphization of monoclinic Nb ₂ O ₅ and its effect on optical properties. Journal of Physics Condensed Matter, 2019, 31, 105401.	0.7	7
48	Porous CoP/C@MCNTs hybrid composite derived from metal–organic frameworks for high-performance lithium-ion batteries. Journal of Materials Science, 2019, 54, 3273-3283.	1.7	29
49	Unraveling the Low-Temperature Redox Behavior of Ultrathin Ceria Nanosheets with Exposed {110} Facets by in Situ XAFS/DRIFTS Utilizing CO as Molecule Probe. Journal of Physical Chemistry C, 2019, 123, 322-333.	1.5	4
50	In situ depth-resolved synchrotron radiation X-ray spectroscopy study of radiation-induced Au deposition. Journal of Synchrotron Radiation, 2019, 26, 1940-1944.	1.0	1
51	Cu(<scp>ii</scp>) sorption by biogenic birnessite produced by <i>Pseudomonas putida</i> strain MnB1: structural differences from abiotic birnessite and its environmental implications. CrystEngComm, 2018, 20, 1361-1374.	1.3	15
52	Bifunctional CO oxidation over Mn-mullite anchored Pt sub-nanoclusters <i>via</i> atomic layer deposition. Chemical Science, 2018, 9, 2469-2473.	3.7	33
53	Superconductivity in Pristine <mml:math <br="" xmlns:mml="http://www.w3.org/1998/Math/MathML">display="inline"><mml:mrow><mml:mn>2</mml:mn><mml:msub><mml:mrow><mml:mi>H</mml:mi>at Ultrahigh Pressure. Physical Review Letters, 2018, 120, 037002.</mml:mrow></mml:msub></mml:mrow></mml:math>	row22.9 mml	:m 10 %> <mm< td=""></mm<>
54	Fabrication of a Singleâ€Atom Platinum Catalyst for the Hydrogen Evolution Reaction: A New Protocol by Utilization of H _{<i>x</i>KKKKKKKK}	1.8	43

#	Article	IF	CITATIONS
55	Selective Passivation of Pt Nanoparticles with Enhanced Sintering Resistance and Activity toward CO Oxidation via Atomic Layer Deposition. ACS Applied Nano Materials, 2018, 1, 522-530.	2.4	47
56	The chemical speciation, spatial distribution and toxicity of mercury from Tibetan medicine Zuotai,β-HgS and HgCl2 in mouse kidney. Journal of Trace Elements in Medicine and Biology, 2018, 45, 104-113.	1.5	19
57	Extracting structural information of higher coordination shells by analyzing EXAFS derivative spectrum. Physica Scripta, 2018, 93, 125701.	1.2	Ο
58	SiO ₂ -protected shell mediated templating synthesis of Fe–N-doped carbon nanofibers and their enhanced oxygen reduction reaction performance. Energy and Environmental Science, 2018, 11, 2208-2215.	15.6	196
59	Effects of Mn average oxidation state on the oxidation behaviors of As(III) and Cr(III) by vernadite. Applied Geochemistry, 2018, 94, 35-45.	1.4	23
60	Oxideâ€Nanotrapâ€Anchored Platinum Nanoparticles with High Activity and Sintering Resistance by Areaâ€Selective Atomic Layer Deposition. Angewandte Chemie - International Edition, 2017, 56, 1648-1652.	7.2	65
61	Oxideâ€Nanotrapâ€Anchored Platinum Nanoparticles with High Activity and Sintering Resistance by Areaâ€Selective Atomic Layer Deposition. Angewandte Chemie, 2017, 129, 1670-1674.	1.6	27
62	Influence of phosphate on phytotoxicity of ceria nanoparticles in an agar medium. Environmental Pollution, 2017, 224, 392-399.	3.7	15
63	The double influence mechanism of pH on arsenic removal by nano zero valent iron: electrostatic interactions and the corrosion of Fe ⁰ . Environmental Science: Nano, 2017, 4, 1544-1552.	2.2	78
64	Discerning lattice and electronic structures in under- and over-doped multiferroic Aurivillius films. Journal of Applied Physics, 2017, 121, 114107.	1.1	6
65	Enhanced removal of roxarsone by Fe ₃ O ₄ @3D graphene nanocomposites: synergistic adsorption and mechanism. Environmental Science: Nano, 2017, 4, 2134-2143.	2.2	89
66	Mechanisms of Synergistic Removal of Low Concentration As(V) by nZVI@Mg(OH) ₂ Nanocomposite. Journal of Physical Chemistry C, 2017, 121, 21411-21419.	1.5	18
67	Nanofence Stabilized Platinum Nanoparticles Catalyst via Facet‣elective Atomic Layer Deposition. Small, 2017, 13, 1700648.	5.2	61
68	Time-resolved XAFS measurement using quick-scanning techniques at BSRF. Journal of Synchrotron Radiation, 2017, 24, 674-678.	1.0	8
69	Confocal depth-resolved fluorescence micro-X-ray absorption spectroscopy for the study of cultural heritage materials: a new mobile endstation at the Beijing Synchrotron Radiation Facility. Journal of Synchrotron Radiation, 2017, 24, 1000-1005.	1.0	11
70	A new technique to measure the differential XAFS spectrum. Chinese Physics C, 2016, 40, 048001.	1.5	1
71	Structural characteristic correlated to the electronic band gap in <mml:math xmlns:mml="http://www.w3.org/1998/Math/MathML"><mml:mrow><mml:mi>Mo</mml:mi><mml:msub><mml:n mathvariant="normal">S<mml:mn>2</mml:mn></mml:n </mml:msub></mml:mrow>. Physical Review B. 2016. 94</mml:math 	ni 1.1	14
72	Sol–gel synthesis and electrochemical properties of c-axis oriented LiCoO ₂ for lithium-ion batteries. RSC Advances, 2015, 5, 51483-51488.	1.7	21

#	Article	IF	CITATIONS
73	Transformation of ceria nanoparticles in cucumber plants is influenced by phosphate. Environmental Pollution, 2015, 198, 8-14.	3.7	84
74	High Co-doping promotes the transition of birnessite layer symmetry from orthogonal to hexagonal. Chemical Geology, 2015, 410, 12-20.	1.4	27
75	Activated-carbon-supported K–Co–Mo catalysts for synthesis of higher alcohols from syngas. Catalysis Science and Technology, 2015, 5, 2925-2934.	2.1	90
76	Optimal azimuthal orientation for Si(111) double-crystal monochromators to achieve the least amount of glitches in the hard X-ray region. Journal of Synchrotron Radiation, 2015, 22, 1147-1150.	1.0	7
77	Introduction of amino groups into acid-resistant MOFs for enhanced U(<scp>vi</scp>) sorption. Journal of Materials Chemistry A, 2015, 3, 525-534.	5.2	378
78	Origin of the different phytotoxicity and biotransformation of cerium and lanthanum oxide nanoparticles in cucumber. Nanotoxicology, 2015, 9, 262-270.	1.6	123
79	In-situ EXAFS study on the thermal decomposition of TiH ₂ . Chinese Physics C, 2014, 38, 038001.	1.5	8
80	Correlating interfacial octahedral rotations with magnetism in (LaMnO3+Î)N/(SrTiO3)N superlattices. Nature Communications, 2014, 5, 4283.	5.8	103
81	Pressure-Induced Valence Change and Semiconductor–Metal Transition in PbCrO ₃ . Journal of Physical Chemistry C, 2014, 118, 23274-23278.	1.5	17
82	Introduction of Bifunctional Groups into Mesoporous Silica for Enhancing Uptake of Thorium(IV) from Aqueous Solution. ACS Applied Materials & Interfaces, 2014, 6, 4786-4796.	4.0	113
83	Ternary composite oxide catalysts CuO/Co3O4–CeO2 with wide temperature-window for the preferential oxidation of CO in H2-rich stream. Chemical Engineering Journal, 2013, 234, 88-98.	6.6	67
84	Iron Isotope Effect and Local Lattice Dynamics in the (Ba, K)Fe2As2 Superconductor Studied by Temperature-Dependent EXAFS. Scientific Reports, 2013, 3, .	1.6	27
85	Influences of the Amorphous Phase on Local Structures and Properties of Ferroelectric Thin Films. Ferroelectrics, 2013, 453, 149-155.	0.3	8
86	Development of pressure-modulated EXAFS method. Chinese Physics C, 2012, 36, 184-187.	1.5	2
87	Study of OSEM with different subsets in grating-based X-ray differential phase-contrast imaging. Analytical and Bioanalytical Chemistry, 2011, 401, 837-844.	1.9	9
88	The measurement of differential EXAFS modulated by high pressure. Journal of Synchrotron Radiation, 2011, 18, 728-732.	1.0	5
89	Quantum critical point in SmO1â^'xFxFeAs and oxygen vacancy induced by high fluorine dopant. Journal of Synchrotron Radiation, 2011, 18, 723-727.	1.0	5
90	A new mobile grazing-incidence X-ray absorption fine spectroscopy endstation at Beijing Synchrotron Radiation Facility. Radiation Detection Technology and Methods, 0, , .	0.4	0